NEOPLASIA
www.neoplasia.com

Volume 20 Number 8 August 2018 pp. 800–812 800

Three Dimensional Mixed-Cell Spheroids Mimic Stroma-Mediated Chemoresistance and Invasive Migration in hepatocellular carcinoma

Iftikhar Ali Khawar[*], Jong Kook Park[†], Eun Sun Jung[‡], Myung Ah Lee[§], Suhwan Chang[¶] and Hyo-Jeong Kuh[#]

[*] Department of Biomedicine & Health Sciences, Graduate School, The Catholic University of Korea, Seoul, Republic of Korea; [†] Department of Biomedical Science, Hallym University, Chuncheon, Republic of Korea; [‡] Department of Hospital Pathology, Seoul St. Mary's Hospital, College of Medicine, The Catholic University of Korea, Seoul, Republic of Korea; [§] Department of Internal Medicine, Seoul St. Mary's Hospital, College of Medicine, The Catholic University of Korea, Seoul, Republic of Korea; [¶] Department of Biomedical Sciences, Asan Medical Center, University of Ulsan College of Medicine, Seoul, Republic of Korea; [#] Department of Medical Life Sciences, College of Medicine, The Catholic University of Korea, Seoul, Republic of Korea

Abstract

Interactions between cancer cells and cancer-associated fibroblasts (CAFs) within the tumor microenvironment (TME) play an important role in promoting the profibrotic microenvironment and epithelial-mesenchymal transition (EMT), resulting in tumor progression and drug resistance in hepatocellular carcinoma (HCC). In the present study, we developed a mixed-cell spheroid model using Huh-7 HCC cells and LX-2 stellate cells to simulate the *in vivo* tumor environment with respect to tumor-CAF interactions. Spheroids were cultured from cancer cells alone (monospheroids) or as a mixture (mixed-cell spheroids) in ultra-low-attachment plates. Compact, well-mixed, and stroma-rich mixed-cell spheroids were successfully established with heterotypic cell-cell contacts shown by the presence of gap junctions and desmosomes. Mixed-cell spheroids showed enhanced expression of collagen type-I (Col-I) and pro-fibrotic factors such as, transforming growth factor beta1 (TGF-β1), and connective tissue growth factor (CTGF) compared to the levels expressed in mono-spheroids. The EMT phenotype was evident in mixed-cell spheroids as shown by the altered expression of E-cadherin and vimentin. Differential drug sensitivity was observed in mixed-cell spheroids, and only sorafenib and oxaliplatin showed dose-dependent antiproliferative effects. Simultaneous treatment with TGF-β inhibitors further improved sorafenib efficacy in the mixed-cell spheroids, indicating the involvement of TGF-β in the mechanism of sorafenib resistance. In 3D matrix invasion assay, mixed-cell spheroids exhibited fibroblast-led collective cell movement. Overall, our results provide evidence that mixed-cell spheroids formed with Huh-7 and LX-2 cells well represent HCC tumors and their TME *in vivo* and hence are useful in studying tumor-stroma interactions as mechanisms associated with drug resistance and increased cell motility.

Neoplasia (2018) 20, 800–812

Introduction

Hepatocellular carcinoma (HCC) is the fifth most frequent cancer and third most common cause of cancer-related mortality worldwide, and the incidence rate is increasing continuously [1]. The treatment modalities include surgical resection, liver transplantation, transarterial

Abbreviations: CTGF, connective tissue growth factor; Col-I, collagen type-I; EMT, epithelial-mesenchymal transition; HCC, hepatocellular carcinoma; HSCs, hepatic stellate cells; TGF-β1, transforming growth factor beta1; TME, tumor microenvironment.

Address all correspondence to: Hyo-Jeong Kuh, Department of Medical Life Sciences, College of Medicine, The Catholic University of Korea, 222 Banpo-daero, Seocho-ku, Seoul 06591, Republic of Korea.
E-mail: hkuh@catholic.ac.kr

Received 2 March 2018; Revised 23 May 2018; Accepted 30 May 2018

1476-5586
https://doi.org/10.1016/j.neo.2018.05.008

chemoembolization, and systemic chemotherapy in patients with advanced HCC. However, conventional chemotherapy cannot be considered a standard-of-care option for advanced-stage HCC due to low survival advantage as demonstrated in a large, randomized trial [2, 3]. HCC is well known for its intrinsic resistance to systemic cytotoxic chemotherapy and local regional therapies [4]. Sorafenib (multikinase inhibitor), the only molecular targeted drug approved for advanced-stage HCC, provides a survival advantage of only 3 months [5]. Such a poor response has been attributed to a number of key factors including abnormal tumor microenvironment (TME), induction of epithelial-mesenchymal transition (EMT), HCC heterogeneity, activation of multiple signaling pathways, and epigenetic dysregulation [6]. Among these factors, TME is being widely studied with respect to its major role in cancer progression and therapeutic resistance [7, 8]. Hence, the TME has been widely utilized as a marker for the identification of novel therapeutic targets and agents, and several TME-targeting drugs are in clinical trials to determine their potential to improve therapeutic efficacy for HCC [9].

The HCC TME comprises cancer and stromal cells, including cancer-associated fibroblasts (CAFs), hepatic stellate cells (HSCs), immune and inflammatory cells, and endothelial cells [10]. CAFs are the crucial components of TME that promote HCC growth and progression by secreting several cytokines and growth factors. CAFs can be derived from different sources such as resident and bone marrow-derived fibroblasts, but HSCs constitute the major source of activated CAFs in the HCC TME [11, 12]. Following activation, HSCs secrete significant amounts of growth factors including transforming growth factor β1 (TGF-β1), connective tissue growth factor (CTGF), and platelet-derived growth factor (PDGF) into the TME. These factors promote activation of both HSCs and HCC cells *via* autocrine and paracrine mechanisms [13, 14]. Bidirectional cancer-stroma activation leads to enhanced cancer cell proliferation, excessive ECM synthesis, EMT and invasion, as well as drug resistance [15]. Targeting HCC-HSC cell interactions has already shown promise for HCC growth suppression in various models; therefore, stellate cells are implicated as a key component of future preclinical drug screening models designed to develop new and effective anti-HCC therapies [14, 16].

Several animal models (ectopic, orthotropic, and genetically engineered) have been developed to study HCC pathogenesis and investigate the outcomes of potential therapies; however, the high cost as well as the prolonged time period required for their implementation and, most importantly, the lack of availability of human fibroblasts limit their usefulness as efficient preclinical models [17]. *In vitro* two-dimensional (2D) co-culture models show the tumor-CAF interactions [18] but lack the potential to accurately mimic the *in vivo* TME; thus, three-dimensional (3D) *in vitro* models have emerged as promising tools for this purpose. Tumor spheroids are now commonly used 3D models, which retain the *in vivo* tumor conditions in terms of morphology, functional phenotype, and specialized microenvironment [19]. These structures exhibit numerous *in vivo* features that make them suitable for use in HCC development studies [20, 21]. 3D co-culture models of liver, breast, and pancreatic cancer established by incorporating cancer and stromal cells have been used to verify the role of stromal cell-mediated phenotypic alterations such as EMT and enhanced mobility that ultimately cause drug resistance [22–25].

In this study, we successfully established a stoma-rich 3D mixed-cell spheroid model by culturing Huh-7 (HCC cell line) and LX-2 (HSCs) cells. We then used this model to demonstrate the role of HSCs in establishing *in vivo*-like HCC TME characteristics including a profibrotic microenvironment and EMT phenotype. The mixed-cell spheroid model was validated by low drug activity and enhanced cell migration. Our findings show that this stroma-rich 3D mixed-cell spheroid model can be considered a clinically relevant *in vitro* HCC tumor model for the investigation of novel stroma-related mechanisms involved in drug resistance and enhanced cell migration and to develop effective anti-HCC therapies.

Materials and Methods

Reagents

Huh-7 cells (HCC cell line) were obtained from the Japanese Collection of Research Bioresources Cell Bank (JCRB), Tokyo, Japan. LX-2 cells (human HSC cell line) were provided by Dr. S. L. Friedman (Mount Sinai School of Medicine, NY, USA). LX-2 cells were developed by spontaneous immortalization of primary HSCs and can be maintained for minimum 50 passages. LX-2 cells showed to express α-SMA, vimentin, and several other profibrotic factors when cultured under low serum conditions [26]. LX-2 cells and Huh-7 cells were maintained in DMEM (Welgene, Daegu, Korea) supplemented with 100 μg/ml streptomycin, 100 U/ml penicillin, 250 ng/ml amphotericin B, and 5% and 10% heat-inactivated fetal bovine serum (Welgene, Daegu, Korea), respectively, in a humidified atmosphere (5% CO_2/95% air) at 37°C. Drugs used in present study include sorafenib (Biovision, CA, USA), oxaliplatin (Hanmi Pharmaceutical, Seoul, Korea), gemcitabine (Korea United Pharm Inc., Seoul, Korea), 5-fluorouracil (5-FU) (Sigma-Aldrich, St. Louis, USA), doxorubicin (Korea United Pharm Inc., Seoul, Korea), TEW-7197 (a TGF-β1 inhibitor, provided by Dr. D.K. Kim, Ewha Womans University, Korea), and pentoxifylline (Sigma-Aldrich). The acid phosphatase (APH) substrate p-nitrophenyl phosphate (PNPP) was obtained from Thermo Fisher Scientific (Rockford, USA). All other chemicals, including the cell tracker PKH26 red fluorescent cell linker kit, were obtained from Sigma-Aldrich unless noted otherwise.

Culture and Analysis of Tumor Spheroids

A liquid overlay technique was used to generate tumor spheroids in 96-well ultra-low-attachment (ULA) plates (Corning, MA, USA). Mixed-cell spheroids were generated by seeding Huh-7 and LX-2 cells at a 1:3 ratio (750: 2250) in ULA plates and incubating for 5 days with daily media changes. Monospheroids were generated by seeding 750 cells of Huh-7 or 2250 cells of LX-2. For mixed-cell spheroids, the mixing ratio of 1:3 (Huh-7: LX-2) was selected based on our preliminary data as well as literature data [27]. For cell tracking experiment, LX-2 cells were stained with cell tracker PKH26 (cell membrane binding dye), prior to mixing with Huh-7 cells, using a standard protocol provided by the manufacturer. The stability of PKH26 loading was confirmed in our preliminary test for cell tracking experiments (data not shown). For preparation of histological sections, spheroids were embedded in OCT compound for cryosections, or fixed in 3.7% formaldehyde and subjected to routine tissue processing for paraffin sections.

Human Tumor Tissue and Xenograft

Clinical study protocols were approved by the Institutional Review Board (project number MC16SISI0027) at the College of Medicine, The Catholic University of Korea. Five tissue samples of human HCC (three HCC and two mixed hepatocellular and

cholangiocarcinoma) were obtained after curative surgical resection during 2011 and 2012 and processed at Department of Pathology, St. Mary's Hospital, The Catholic University of Korea. Tissues were immediately fixed in 10% neutral buffered formalin for 4 to 8 hours depending on the sample size and were subjected to routine paraffin-embedding protocols [28]. Animal experiment protocols were approved by the Institutional Animal Care and Use Committee (project number CUMC2015-0046-02) at the College of Medicine, The Catholic University of Korea. Male BALB/c mice (aged 4 weeks) were purchased from Orient Bio Inc. (Seongnam-si, Gyeonggi-do, Korea). For HCC xenograft, Huh-7 cells were harvested during log phase, and 10^7 viable cells suspended in phosphate-buffered saline (PBS) were subcutaneously injected into the right flank of animals [29]. Tumor tissues were harvested after 3-4 weeks for histological and immunohistochemical staining.

Scanning Electron Microscope (SEM) and Transmission Electron Microscope (TEM)

For both SEM and TEM observations, spheroids were processed by standard fixation and embedding procedures. For TEM images, ultrathin sections were examined using a JEM 1010 (Japan) equipped with a CCD camera (SC1000, Gatan, USA). For SEM images, samples were additionally coated with gold and examined using a JSM-5410LV microscope (JEOL, Japan).

Immunofluorescence and Immunohistochemical Staining of Tumor Spheroids and In Vivo Tissues

Formalin-fixed, paraffin-embedded (FFPE) sections of tumor spheroids, human HCC tissues, and xenograft tumor tissues were immunostained for hypoxia inducible factor-1 alpha (HIF-1α) (1:100, H-206, Santa Cruz, Dallas, TX, USA), alpha smooth muscle actin (α-SMA) (1:100, ab5694, Abcam, Cambridge, UK), Collagen type I (Col-I) (1:100, ab34710, Abcam), TGF-β1 (1:100, ab66043, Abcam), CTGF (1:100, ab6992, Abcam), E-cadherin (1:200, 3195S, Cell Signaling, Danvers, MA, USA), vimentin (1:250, ab92547, Abcam), Ki-67 (1:100, sc-15,402, Santa Cruz), and cleaved-PARP (c-PARP) (1:100, ab32561, Abcam) at 4°C overnight in a humidified chamber. After secondary antibody (1:500, R37117, Thermo Fisher) and DAPI treatment (1:1000, D9564, Sigma-Aldrich), sections were mounted and visualized by confocal microscopy (LSM 510 Meta, Zeiss, Oberkochen, Germany). The relative fluorescence intensity was calculated by normalizing antigen intensity to DAPI. By normalizing to DAPI which represents total number of cells, quantitative comparison was made between spheroids with different cell number. For immunohistochemical detection, slides were washed after primary antibody treatment, incubated in 0.3% hydrogen peroxide, and visualized by Dako EnVisionTM detection system. Slides were then counterstained with hematoxylin and mounted. Final images of samples were acquired using slide scanner (Pannoramic MIDI, 3D HISTECH, Hungary).

Drug Response Assay

Stock solutions of sorafenib and TEW-7197 were prepared in DMSO and stored at −20°C for up to 1 month. Doxorubicin, oxaliplatin, gemcitabine, 5-FU, and pentoxifylline were freshly prepared before use in normal saline. All drugs were diluted in culture media containing <0.1% DMSO and <10% saline. For drug exposure, spheroids were incubated in drug-containing media for 48 hours without media change. For drug combination, agents were given simultaneously at predetermined concentrations. After drugs treatment, spheroids were washed in PBS and transferred to a 96-well flat-bottom plate for viability assay. Cells viability was determined using APH assay [30]. Briefly, spheroids were incubated with 100 µl of assay buffer (0.1 M sodium acetate, 0.1% Triton-X100 in deionized water supplemented with PNPP) at 37°C for 90 minutes. The reaction was stopped by adding 10 µl of 0.1 N NaOH, and absorbance was measured at 405 nm (BioTek, Winooski, VT, USA) within 15 minutes. Dose-response curve was analyzed to calculate IC_{50} using Emax model [31]. Drug combination effect was analyzed by comparing the sum of fraction affected from each agent to the fraction from the combination. Drug exposure time was not extended beyond 48 hours because prolonged drug exposure or delayed harvest compromised integrity or compactness of spheroids, causing cell loss during transfer step. For drug penetration assay, spheroids were treated with doxorubicin (10 µM) for 6, 12, and 24 hours, and cryosections of spheroids were prepared using O.C.T compound. Doxorubicin autofluorescence was detected by confocal microscope.

Invasion Assay

Cell motility was determined using Matrigel (Cat. No. 354234; Corning Incorporated) and collagen (rat tail, BD Biosciences) invasion assay according to a previously described protocol [32]. Collagen gel solution (2 mg/ml) was prepared by mixing collagen with phenol red–containing PBS and pH adjusted to 7.4 using 0.5 N NaOH. Each well of a 96-well plate was coated with 100 µl of Matrigel or collagen (1 hour at 37°C) and filled with 100 µl of media. Spheroids cultured for 5 days were placed on the matrix and monitored for cell invasion under a microscope after 24, 48, and 72 hours. ImageJ software was used to measure the area covered by cells, and percent changes were calculated with respect to the area measured in the absence of matrix. For fluorescence image analysis, Huh-7 cells were stained with PKH26 dye prior to mixing with LX-2 cells and cultured for 5 days to form mixed-cell spheroids, followed by DAPI staining. The confocal optical sections were captured at 5-µm interval, and 45 sections were stacked into a *z*-projection.

Statistical Analysis

All data were expressed as the mean ± standard error (SE) from three or more independent experiments. Student's *t* test as well as analysis of variance (ANOVA), followed by Tukey's test, was used to test the statistical significance using Microsoft Excel 2010 and SPSS version 24 (SPSS Inc., Chicago, IL, USA). $P < .05$ was considered to indicate statistical significance.

Results

Characteristics of 3D Mixed-Cell Spheroids of LX-2 and Huh-7 Cells

LX-2 and Huh-7 cells at a seeding density of 2250 and 750 cells, respectively, were cultured alone or as a mixed suspension at a seeding density of 3000 cells (LX-2: Huh-7 = 2250:750) in 96-well ULA plates. Growth and morphology of spheroids were monitored according to size and compactness for up to 5 days. LX-2 cells formed spheroids of approximately 350 µm in diameter by day 1 and showed no increase in size over time (Figure 1*A*). With cell viability maintained, the opacity of spheroids increased until 14 days (data not shown), indicating increased compactness. Huh-7 cells showed rapid 3D growth, starting as loose clusters after 1 day of culture to fully formed compact spheroids (diameter 430 µm) after 5 days (Figure 1*A*). Mixed-cell spheroids of LX-2 and Huh-7 cells showed rapid growth similar to that of Huh-7 monospheroids (Figure 1*A*), indicating no growth-inhibitory effect to

each other when co-cultured. All three types of spheroids showed sufficient compactness and stability for use in further experiments.

The 3D assembly of cells and subcellular structures were examined by SEM and TEM. While LX-2 monospheroids showed a smooth surface, Huh-7 monospheroids had a rough surface with a bulging arrangement of individual cells. A smooth cell surface and compact cellular organization were seen in the mixed-cell spheroids (Figure 1*B* and Supplementary Figure 1). Cells in the peripheral region of LX-2 and Huh-7 monospheroids showed an elongated spindle shape with significant membrane ruffling (Figure 1*B*). At the periphery of mixed-cell spheroids, both types of cells showed extensive membrane protrusions (filopodium), suggesting the presence of actin-driven invadosome formation. Cell-cell contacts were demonstrated by the presence of gap junctions, desmosomes, and microvilli in LX-2 monospheroids and mixed-cell spheroids, while only gap junctions and microvilli were observed in the Huh-7 monospheroids (Figure 1*B*). A few necrotic cells were seen in the core region of monospheroids and mixed-cell spheroids indicating the quiescent and necrotic state of the innermost cells. Typical subcellular structures formed by Huh-7 and LX-2 cells that were observed in monospheroids were also identified in mixed-cell spheroids. For example, Huh-7 cells showed a large nucleus with euchromatin as the predominant chromatin structure, while LX-2 cells possessed a relatively small nucleus with high levels of heterochromatin. Glycogen particles were only seen in Huh-7 cells, while fat particles were abundant in LX-2 cells (Figure 1*B*, Supplementary Figure 1, and Supplementary Table 1). The presence of these typical ultrastructures shows the active transcriptional and metabolic status of the cells in the mixed-cell spheroids model.

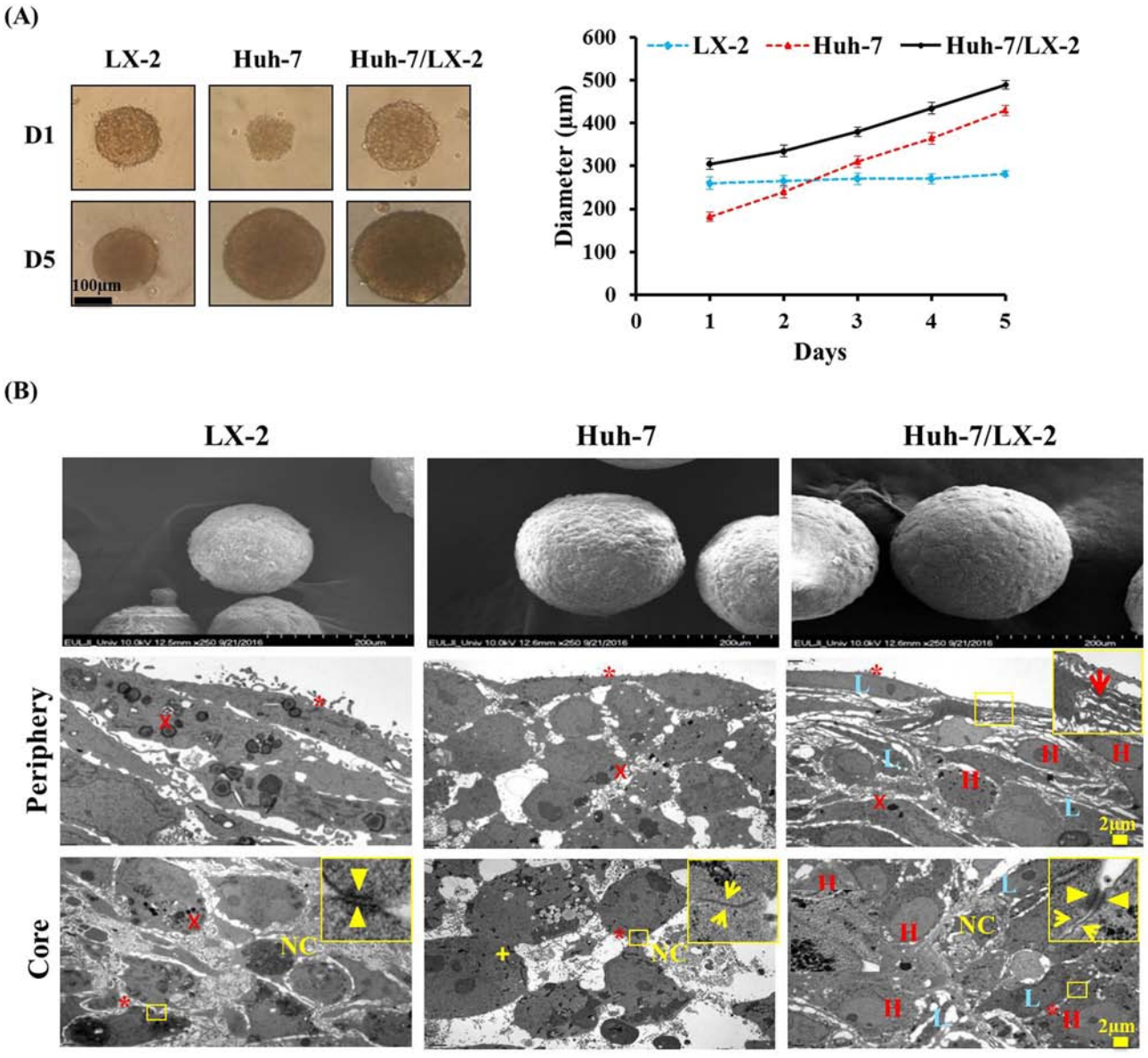

Figure 1. Morphological characteristics of 3D mixed-cell spheroids. (A) HCC cells (Huh-7) and HSCs (LX-2) were seeded alone (monospheroids) or in mixture (1:3 ratios, mixed-cell spheroids) and monitored for 3D growth during 5 days of culture. Scale bar, 100 μm. (B) SEM and TEM images of mono- and mixed-cell spheroids at day 5 show peripheral cytoplasmic protrusions (red arrow) and subcellular structures containing cell-cell interactions: microvilli (*), gap junctions (yellow arrows), and desmosomes (yellow arrow heads). Scale bar, 2 μm. H, Huh-7; L, LX-2; NC, necrotic cell; X, fat particles; +, glycogen particles.

Distribution of HSC and Its Fibrogenic Effect in 3D Mixed-Cell Spheroids

Fluorescence tracking of LX-2 cells in 3D mixed-cell spheroids demonstrated a well-mixed distribution of both types of cells (Figure 2*A*). LX-2 cells constituted a larger proportion of cells until day 3, then assumed an almost equal fraction by day 5 due to outgrowth of Huh-7 cells. Relative localization of LX-2 (labeled) cells in the central region was observed, which can be attributed to the preferential proliferation of cancer cells compared to LX-2 cells in the periphery.

The hypoxic condition was demonstrated by HIF-1α expression in the core region of mixed-cell spheroids (Figure 2*B*). In the mixed-cell spheroids, not only α-SMA but also Col-I and profibrotic cytokines

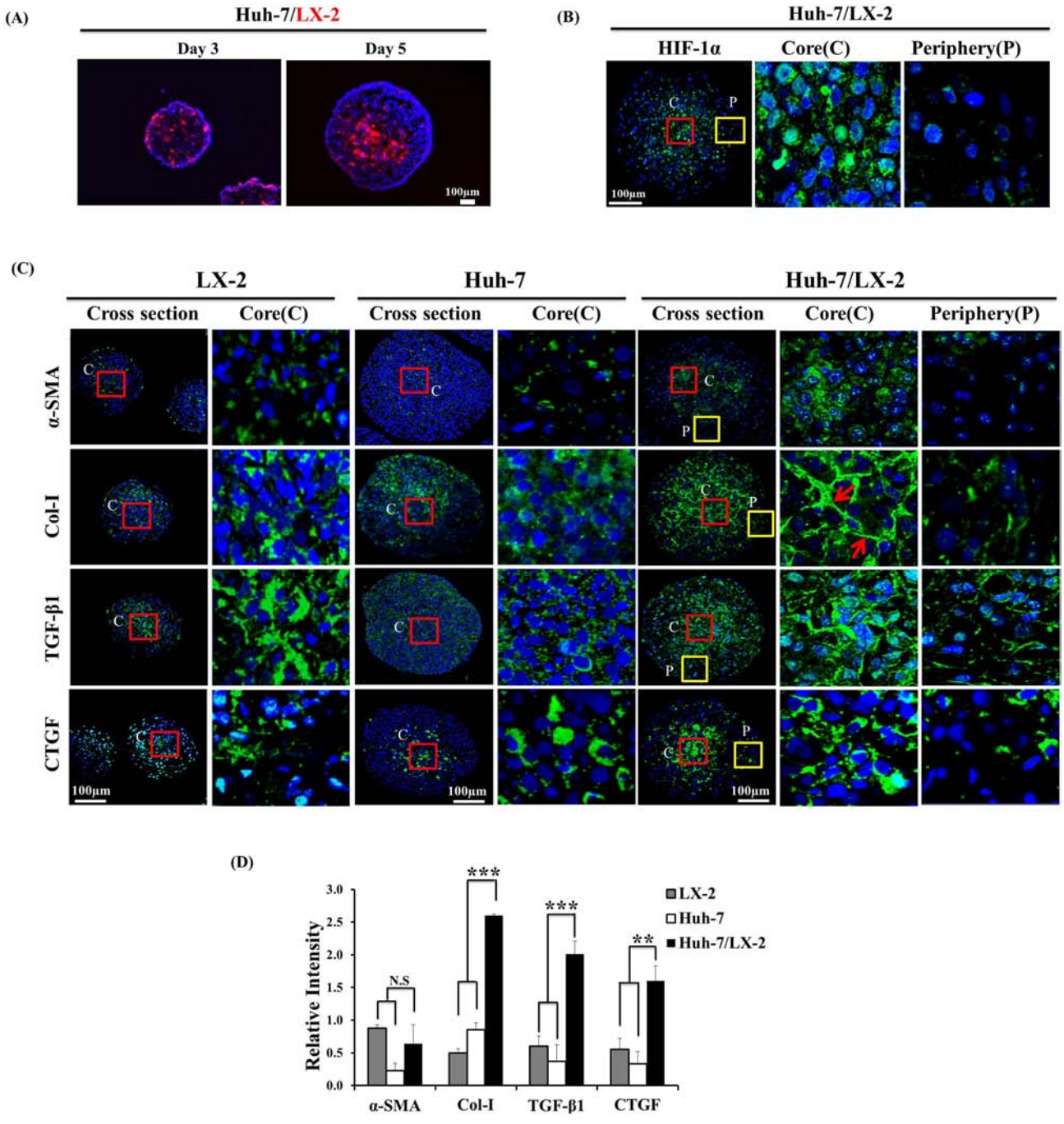

Figure 2. Distribution of LX-2 cells and stromal activation markers in 3D mixed-cell spheroids. (A) LX-2 cells were labeled with PKH26 tracer (red fluorescence) prior to mixing with Huh-7 cells. Cryosections of mixed-cell spheroids cultured for 3 and 5 days were prepared for fluorescence imaging. Counterstain, DAPI (blue). Scale bar, 100 μm. (B) The expression of HIF-1α was detected in mixed-cell spheroids after 5 days of culture using immunofluorescence staining. (C) The expression of α-SMA, Col-I, TGF-β1, and CTGF was detected in LX-2 and Huh-7 monospheroids and mixed-cell spheroids after 5 days of culture. (D) Relative fluorescence intensity of stained biomarkers in cross-sections of monospheroids and mixed-cell spheroids after 5 days. Scale bar, 100 μm. Arrows, fibrillar Col-I arrangement. Relative intensity was calculated by normalizing staining intensity to DAPI (blue) and expressed as mean ± SE of more than five replicates. N.s. = no significance, $^{**}P < .005$ and $^{***}P < .001$ (by one-way ANOVA) relative to sum of monospheroids.

TGF-β1 and CTGF showed elevated expression level in the core region of mixed-cell spheroids where LX-2 cells were preferentially localized compared to the periphery (Figure 2, *A* and *C*). It indicated that LX-2 cells were responsible for the expression of these profibrotic cytokines and collagen accumulation. Co-stimulatory interaction between Huh-7 and LX-2 cells was demonstrated by the increased level of Col-I with fibrillar morphology in mixed-cell spheroids compared to either type of monospheroids (Figure 2, *C* and *D*). Expression of TGF-β1 and CTGF was also increased significantly in mixed-cell spheroids compared to that in either monospheroid (Figure 2*D*).

The Mixed-Cell Spheroid Model Mimics Major Features of In Vivo HCC Tumors

Expression of Col-I and profibrotic factors was detected in mixed-cell spheroids and tumors obtained from human HCC patients as well as in human xenografts. The comparative analysis showed thick fibrous septa in human and xenograft tumors, which are characteristic of a stroma-rich environment and corresponded to an abundant stroma region (eosinophilic) in mixed-cell spheroids (Figure 3). Dense α-SMA expression was found both in tumors from HCC patients and human xenografts as well as in the mixed-cell spheroids. Fibrillar Col-1 expression in mixed-cell spheroids appeared similar to the thick bundles of collagen fibers found in tumors from HCC patients and human xenografts. Significant levels of TGF-β1 and CTGF expression in tumors from HCC patients and human xenografts were also comparable to those in the mixed-cell spheroids (Figure 3, Supplementary Figure 2). Overall, these results indicated the validity of our mixed-cell spheroids as a stroma-rich 3D *in vitro* model of tumors from HCC patients and human xenografts.

EMT-Like Phenotype in 3D Mixed-Cell Spheroids

The effect of stellate cell co-culture on the expression of EMT markers was examined in Huh-7/LX-2 co-spheroids. LX-2 monospheroids showed typical mesenchymal phenotype such as lack of epithelial marker E-cadherin and enhanced expression of vimentin, a mesenchymal marker. In Huh-7 monospheroids, basal level expression of the E-cadherin was observed, whereas expression of vimentin was very low (Figure 4*A*). Following co-culture with LX-2 cells, significantly decreased E-cadherin expression and increased vimentin expression were observed, indicating the existence of EMT-like phenotypic changes induced by HSC co-culture. Decreased E-cadherin expression in mixed-cell spheroids was prominent in the periphery, with the residual expression restricted to the inner core of the mixed-cell spheroids. Vimentin expression appeared as patches of dense staining throughout the mixed-cell spheroids, not restricted to the core region where LX-2 cells were localized (Figure 2*A*). Vimentin expression detected in Huh-7 cells in the periphery clearly indicates that cell-cell interaction inducing EMT was present in our mixed-cell spheroids (Figure 4*A*). Similar patterns of E-cadherin and vimentin expression were detected among Huh-7/LX-2 mixed-cell spheroids, HCC patient tumors, and human xenograft tumors (Figure 4*B*). These results provide evidence of the significant level of *in vivo* mimicry of Huh-7/LX-2 mixed-cell spheroids and the role of HSC with regard to the EMT phenotype.

Drug Resistance in 3D Mixed-Cell Spheroids

Sorafenib sensitivity of Huh-7 and LX-2 cells was compared when cells were cultured as 2D monolayers and 3D spheroids. Two-fold increase in sorafenib IC_{50} was observed in Huh-7 cells cultured as 3D spheroids compared to 2D (11.5 μM *vs.* 5.31 μM), indicating reduced sensitivity to sorafenib (Figure 5*A*). No difference in IC_{50} was shown in LX-2 cells between 2D and 3D (13.7 μM and 14.6 μM). Mixed-cell spheroids showed a differential sensitivity to anticancer drugs with a rank order of sorafenib > oxaliplatin >> 5-FU > gemcitabine. Growth inhibition by 50% was obtained for sorafenib and oxaliplatin at 24.8 μM and 84.6 μM, respectively, while 5-FU and gemcitabine did not show significant activity even up to 300 μM (Figure 5*B*). Importantly, the sensitivity of Huh-7 cells to sorafenib decreased when co-cultured with HSC as indicated by the increased IC_{50} value from 11.5 μM in Huh-7 monospheroids to 24.8 μM in the mixed-cell spheroids (Figure 5, *A* and *B*). The effect of sorafenib (20 μM) was enhanced when combined with TGF-β1 inhibitors such as TEW-7197 (10 μM) or pentoxifylline (100 μM) in an additive manner (Figure 5*C*). For combined treatment, 10-fold higher dose of TEW-7197 was utilized than previously reported concentration in monolayer HCC cells [33, 34], while pentoxifylline concentration was determined based on our preliminary drug activity evaluation experiments. Enhanced efficacy after combined treatment with sorafenib and TGF-β inhibitor TEW-7197 was also demonstrated by the significantly increased level of drug-induced apoptosis detected by increased c-PARP expression, while there were no significant changes in expression of the proliferative maker, Ki-67 (Figure 5*D*).

Invasive Migration of Cells Out of 3D Mixed-Cell Spheroids

Invasive migration of cells from 3D spheroids was evaluated by culturing 5-day-old spheroids in Matrigel or collagen-coated wells. Huh-7 cells in monospheroids did not show invasion even after 72 hours, whereas LX-2 cells showed radial extension of cell strands out of monospheroids (Figure 6*A*, Supplementary Figure 3). Cell migration out of mixed-cell spheroids showed a radial invasion into the surrounding matrix producing a characteristic "starburst" invasion pattern in a time-dependent manner (Figure 6*B*, Supplementary Figure 3). Enhanced cell migration out of mixed-cell spheroids resulted in large number of detached cells away from the spheroids with 40% increase in cell-covered area when incubated on the Matrigel compared to control of no matrix (Figure 6*B*). No cell migration out of mixed-cell spheroids without matrix, either Matrigel or collagen, suggested that invasive migratory activity of Huh-7 and LX-2 cells may require additional stimuli provided by matrix. Migration of cancer cells from mixed-cell spheroids was traced by labeling Huh-7 cells with a fluorescent dye prior to spheroid formation to detect HSC-induced cancer cells invasion. LX-2 cells appeared to function as the "leader cells," with matrix invasion observed after 24 hours in culture, while Huh-7 cells were found only at the spheroid boundary at this time point. Huh-7 cells appeared to function as follower cells," with migrating cells observed after 48 hours in culture followed by an identical migration pattern observed after 72 hours (Figure 6*C*). The labeled Huh-7 cells were dispersed around spheroids and found to be coupled to nonlabeled cells, indicating a collective migration of Huh-7 cells with LX-2 cells *via* cancer-stroma cross talk.

Discussion

In the present study, we developed and characterized 3D mixed-cell spheroids prepared from human HCC cells and HSCs as a clinically relevant model for the evaluation of drug activity and cell migration.

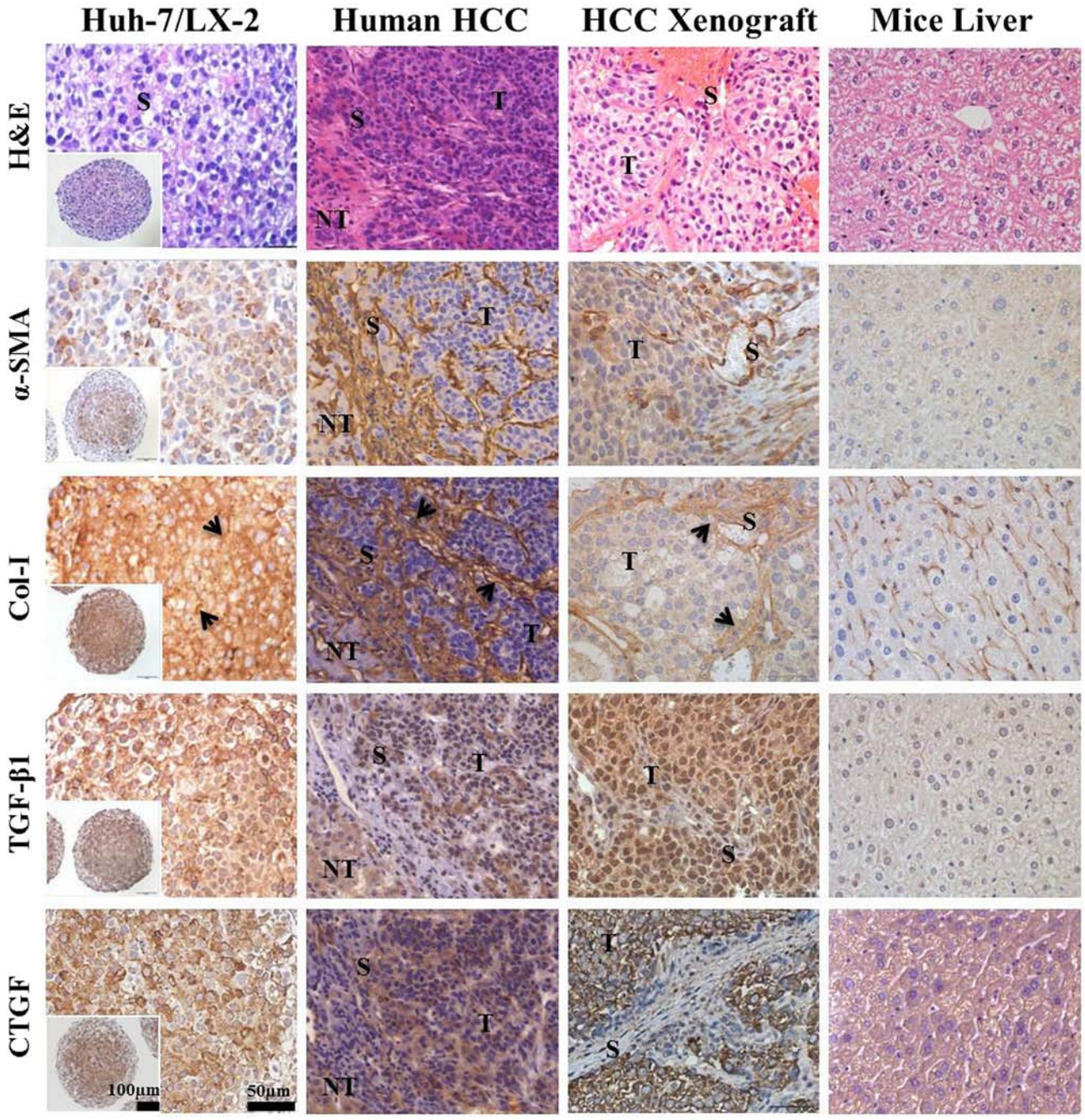

Figure 3. Immunohistological comparison of stromal biomarkers in Huh-7/LX-2 mixed-cell spheroids with human HCC tumors and Huh-7 xenograft. Human tumor samples were obtained from FFPE archives of patients (see methods for details). Huh-7 xenografts were obtained 4 weeks after subcutaneous injection male Balb/c mice with 1×10^7 cells. H&E staining and immunohistological detection of α-SMA, Col-I, TGF-β1, and CTGF expression in paraffin sections of mixed-cell spheroids, human HCC and xenograft tissues, and normal mice liver. All the antibodies show specificity against human and mouse antigen. Scale bars, 100 μm (inset) and 50 μm. T, tumor region; NT, nontumor region; S, stroma region; arrows, fibrillar Col-I arrangement.

Both of these cell lines closely reflect the *in vivo* characteristics of the stroma-rich HCC TME. For example, Huh-7 is a well-established HCC cell line showing a very close resemblance to human HCC tissues [35–37]. LX-2 is a human HSC cell line expressing several profibrotic factors that make it suitable for culture as a model of the desmoplastic human HCC microenvironment [26]. Thus, the characteristics of these cells potentiate their use in the investigation of direct HCC-HSC interactions.

The plating ratio of Huh-7 and LX-2 cells (1:3) was chosen to produce stroma-rich spheroids after 5 days of culture, and a well-mixed cell population with almost equivalent fractions of both cell types was seen in the spheroids (Figures 1*B* and 2*A*). The majority of LX-2 cells were localized in the central core region, although small fractions of cells were also seen in the outer peripheral layers (Figure 2*A*). In contrast, when fibroblasts were mixed with HepG2 cells to form spheroids, cells were spatially segregated resulting in localization of fibroblasts only in

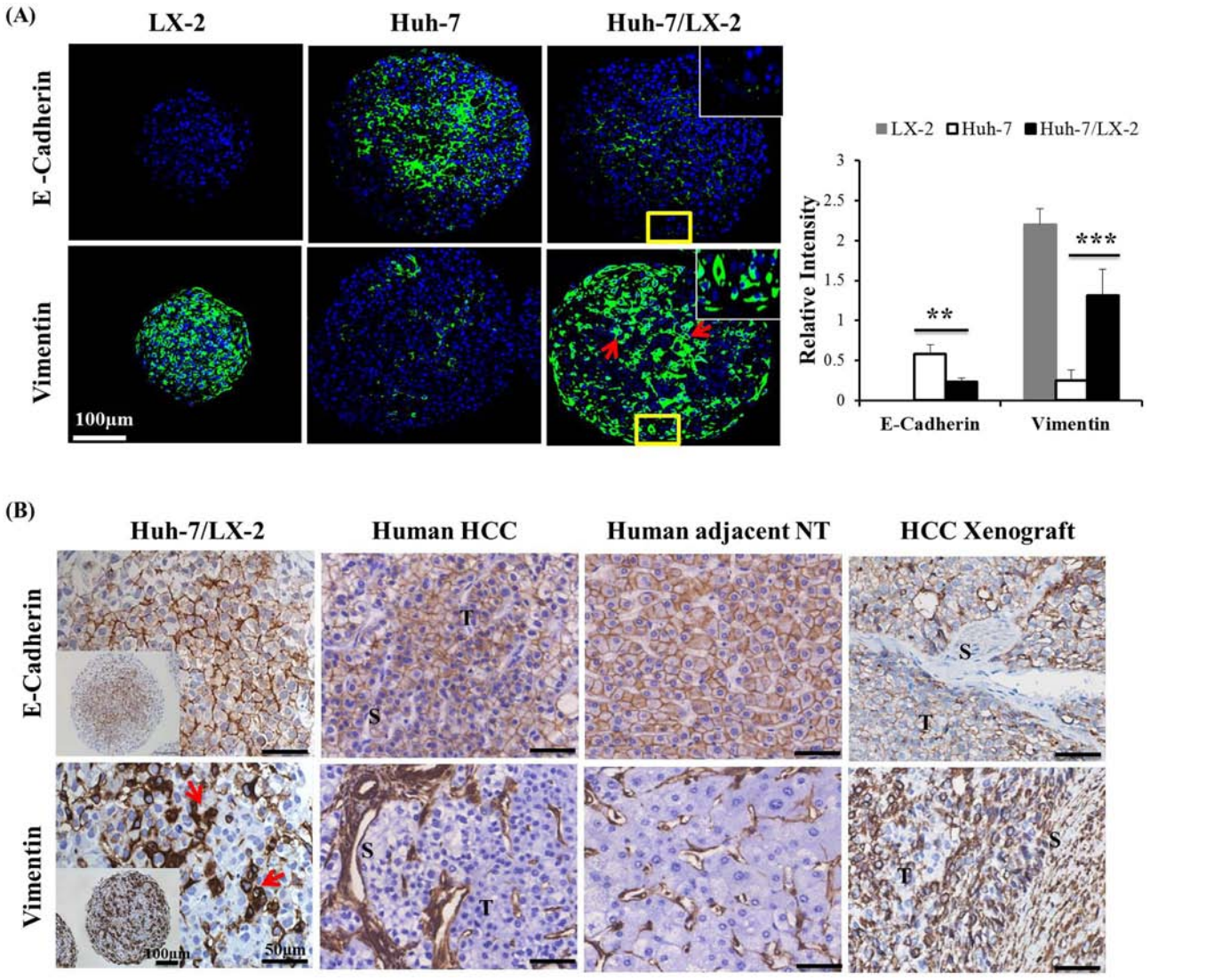

Figure 4. Expression of EMT markers in mixed-cell spheroids and *in vivo* tissues. (A) The expression of the EMT markers E-cadherin and vimentin was detected by immunofluorescence staining of paraffin sections of LX-2 and Huh-7 monospheroids and mixed-cell spheroids. Counterstain, DAPI (blue). Scale bars, 100 μm. Relative intensity across sections was expressed as mean ± SE of more than five replicates. $^{**}P < .005$ and $^{***}P < .001$ relative to Huh-7 monospheroids. (B) Comparison of EMT marker expression in Huh-7/LX-2 mixed-cell spheroids with that in paraffin sections of human HCC and adjacent nontumor (NT), and HCC xenograft tissue samples. All the antibodies show specificity against human and mouse antigen. Scale bars, 100 μm (inset) and 50 μm. T, tumor region; S, stroma region; arrows, expression in patches.

the central region as reported by Song et al. and Yip et al. [22, 38]. Therefore, we believe that the HCC-HSC interactions observed both in the core as well as in the peripheral region of mixed-cell spheroids are similar to those that occur under *in vivo* conditions [12]. 3D spheroids developed without matrix encapsulation method facilitate direct cell-cell interactions *via* paracrine and contact-mediated mechanisms. These interactions were demonstrated by the presence of gap junctions and desmosomes between HCC-HSCs. The characteristic subcellular structures were also preserved in 3D spheroids as shown by chromatin, fat, and glycogen particles (Figure 1*B* and Supplementary Figure 1*B*). However, scaffold-based 3D spheroids formed in polymeric biomaterials (collagen, Matrigel *etc.*) may hinder contact-mediated cell-cell interactions, and unexpected factors derived from the matrix may negatively affect these interactions [39].

Stromal cells are known to be activated under hypoxia, which is a hallmark of HCC growth and progression. This promotes cancer cell survival by supporting cellular adaption to hypoxic microenvironments and the development of drug resistance [40, 41]. Hypoxia-induced HSC activation was confirmed by HIF-1α and α-SMA expression in the core region of mixed-cell spheroids, where the majority of LX-2 cells were localized (Figure 2). After activation, HSCs secrete various paracrine factors, such as TGF-β1 and its downstream mediator, CTGF, as well as vascular-derived growth factor (VEGF) and PDGF, which not only are potent fibrogenic factors (autocrine and paracrine) but also maintain their activation [42].

The elevated levels of α-SMA, Col-I, and profibrotic cytokines (both HSCs and hepatoma cells) have been related with HCC growth and progression [43–45]. The *in vivo* phenotypic similarity of our stroma-rich mixed-cell spheroid model was confirmed by marked expression of α-SMA, Col-I, and profibrotic factors, shown at a comparable level to that in tumors from HCC patients as well as human xenograft (Figure 3 and Supplementary Figure 2). Expression

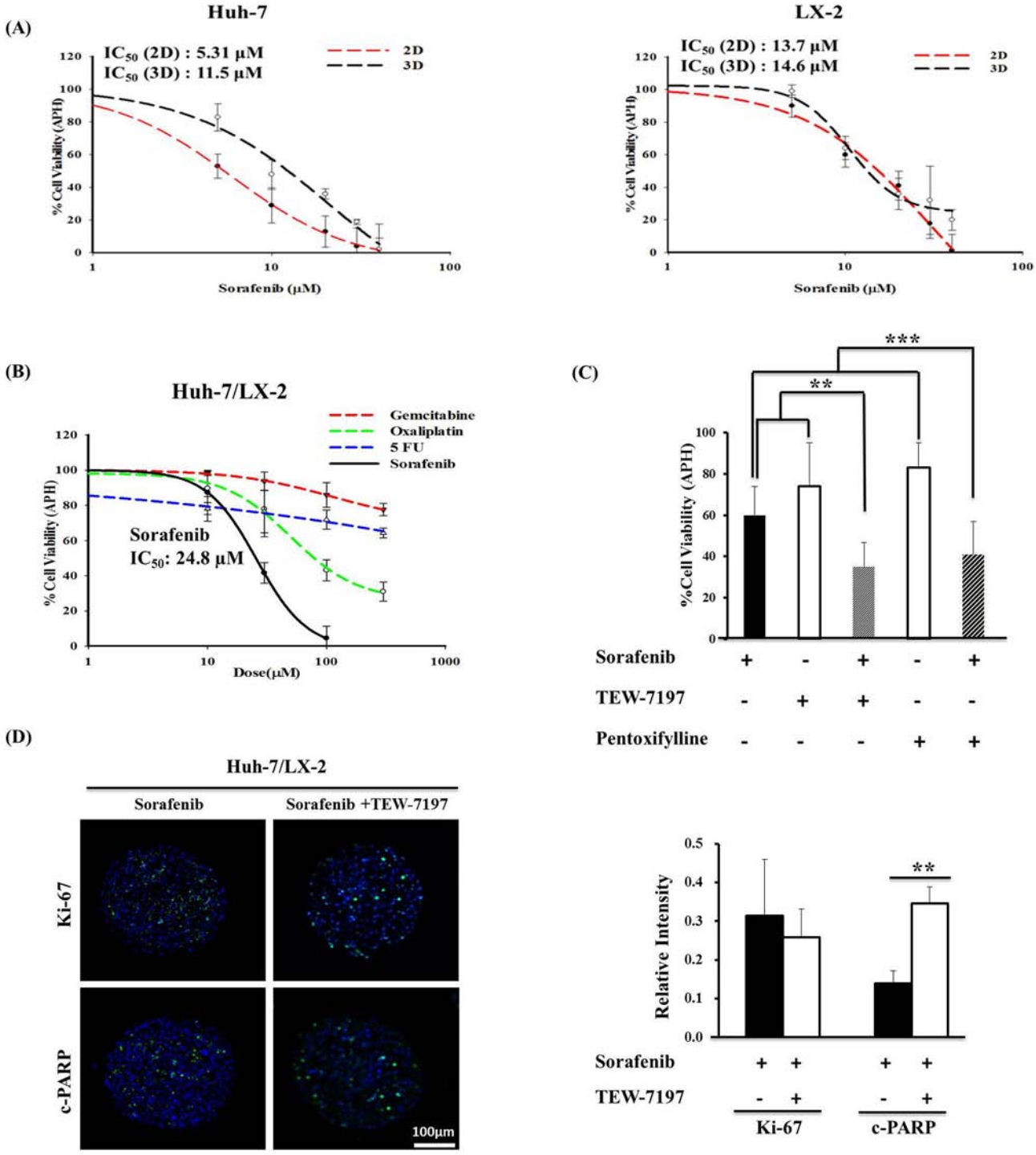

Figure 5. Anticancer drug response. (A) Comparison of sorafenib sensitivity of Huh-7 and LX-2 cells cultured under 2D and 3D conditions. Cells were exposed to different concentrations of sorafenib (5, 10, 20, 30, and 40 μM) for 48 hours, and cell viability was analyzed by APH assay. (B) Spheroids were cultured for 5 days and exposed to media containing drugs (10, 30, 100, and 300 μM) for 48 hours, and drug activity was detected by APH assay. (C) Reduced cell viability in mixed-cell spheroids was observed after combined treatment of sorafenib (20 μM) with TEW-7197 (10 μM) or pentoxifylline (100 μM). Data are expressed as mean ± SE of more than five replicates from three or more independent experiments. $^{**}P < .005$ and $^{***}P < .001$ (by one-way ANOVA) relative to sum of single-agent treatment. (D) Changes in the expression levels of Ki-67 and c-PARP in mixed-cell spheroids after combined treatment with sorafenib and TEW-7197. Counterstain, DAPI (blue). Scale bars, 100 μm. $^{**}P < .005$ relative to single-agent treatment.

of α-SMA and Col-I in human HCC tumors and human xenograft (Figure 3) was highly restricted to the stroma regions. In xenograft tumors, α-SMA and Col-I expression can be mainly attributed to mouse stromal cells recruitment and activation in the tumor area, with minor contribution from inoculated human cancer cells (Figures 2*B* and 3). Normal mouse liver tissue showed lack of reactive stromal cells as

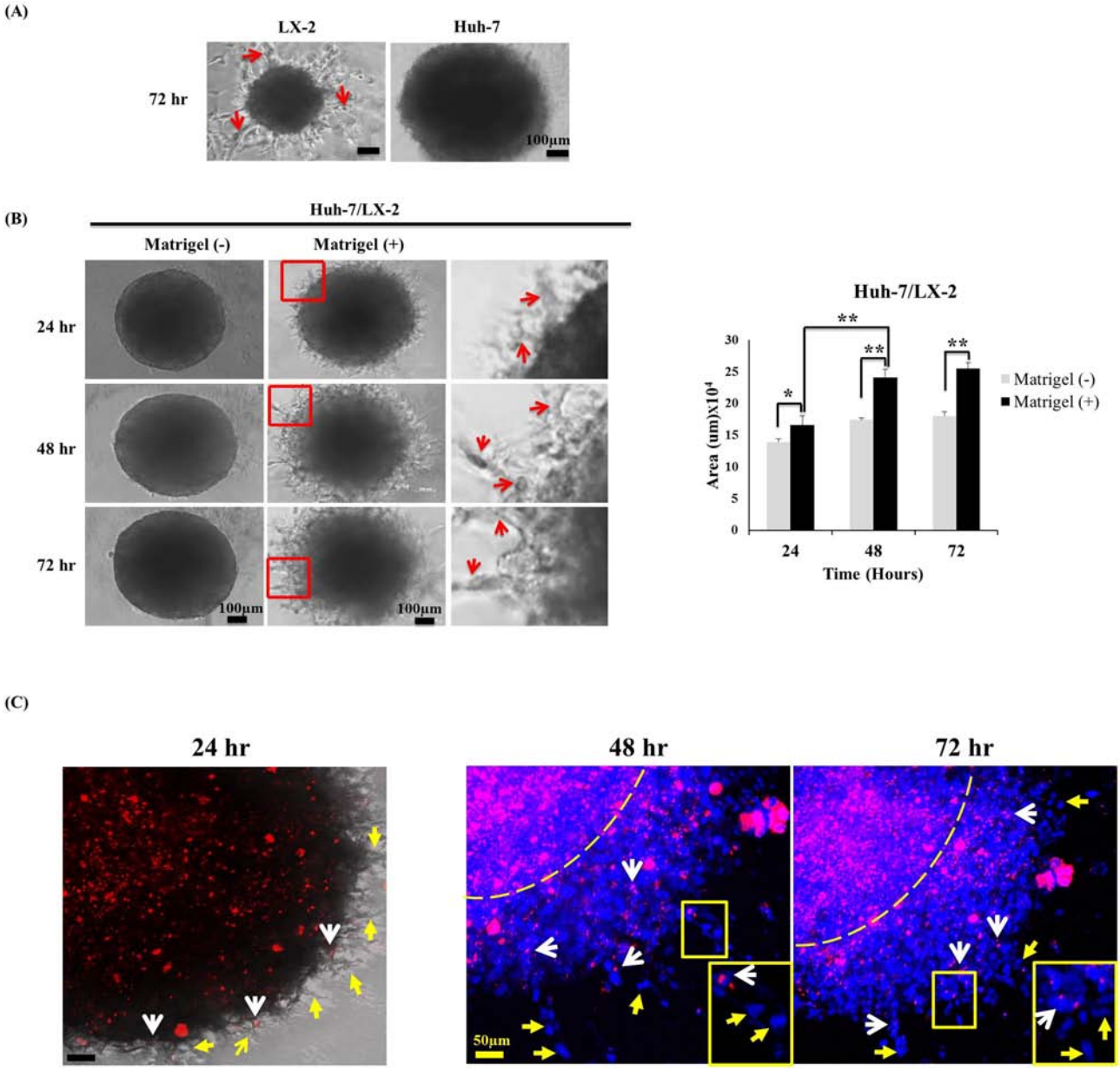

Figure 6. Invasive migratory profile of mixed-cell spheroids. (A) Cell invasion and migration from monospheroids embedded in Matrigel for 72 hours. Scale bar, 100 μm. (B) In mixed-cell spheroids, small cellular protrusions with invadosomes were visible after 24 hours that continuously extended into the matrix over 72 hours. The relative invasion area was quantified using ImageJ software. Scale bars, 100 μm. *P < .05 and **P < .005. (C) Fluorescence dye tracing of Huh-7 cells (PKH26: red) to show migration from mixed-cell spheroids. Red arrows, invadosome; white arrows, PKH26-labeled Huh-7 cells; yellow arrows, DAPI-stained (blue) LX-2 cells; dotted line, spheroid margin. Scale bar, 50 μm.

demonstrated by absence of α-SMA and basal level Col-I expression (Figure 3). Human stromal cells are not well sustained when inoculated in mice; instead, they are replaced by stromal cells of mouse origin, *e.g.*, patient-derived xenograft tumors showed replacement of 75% human stromal cells after 4 weeks of inoculation [46, 47]. Activated HSCs play critical roles in EMT induction by secreting various growth factors in HCC [15, 48]. Hence, our 3D stroma-rich mixed-cell spheroid model may provide HCC-HSC interactions occur *via* juxtacrine and paracrine mechanisms and accurately mimic the *in vivo* conditions of the profibrotic microenvironment.

In accordance with the activated status of HSCs (Figure 2*B*), EMT-related phenotypic changes, such as altered E-cadherin and vimentin expression, were also observed in our mixed-cell spheroids (Figure 4*A*). Similar phenotypic patterns were also seen in the tumors from HCC patients and human xenografts (Figure 4*B*). EMT-related phenotypic changes accompanied by upregulated expression of TGF-β/CTGF in mixed-cell spheroids strongly suggest TGF-β/CTGF-mediated signaling for EMT induction in our model (Figures 2*C* and 4). TGF-β-induced EMT phenotype has also been reported in 3D HCC organoids and HCC tissues [20, 43]. As a potent inducer of EMT, TGF-β regulates the expression of various EMT-promoting factors *via* the Smad/non-Smad signaling pathway [49, 50]. Preliminary results from early trials showed that TGF-β inhibition improves clinical outcome with reduction of EMT [49]. Cell

type–specific involvements as well as TGF-β/CTGF-mediated mechanism in EMT induction using *in vivo* mimic 3D spheroids warrant further investigation.

Currently, 3D tumor spheroids are more widely utilized for *in vitro* drug testing than the conventional 2D culture models in which cancer cells usually show higher drug sensitivity [51–53]. We observed decreased sensitivity to sorafenib in Huh-7 spheroids than in cells grown as 2D monolayers (Figure 5*A*). Similar resistance to sorafenib has been reported in another study using 3D culture of Huh-7 cells [54]. The oxaliplatin sensitivity observed in our model is consistent with known antiproliferative and apoptotic activity obtained in other preclinical *in vitro* and *in vivo* models [55] and has recently been suggested as a new treatment option in advanced HCC [56]. Mixed-cell spheroids showed lower sensitivity to sorafenib (IC_{50}, 24.8 μM) than the Huh-7 monospheroids (IC_{50}, 11.5 μM) (Figure 5, *A* and *B*). The two-fold increased IC_{50} in mixed-cell spheroids indicated the induction of HSC-mediated resistance to sorafenib. Reduced drug penetration has been reported in desmoplastic tumors with quantitative and qualitative changes in ECM [8]. Our mixed-cell spheroids showed an increased expression and desmoplastic remodeling of collagen matrix (Figure 2*C*), which may be associated with reduced penetration of doxorubicin (Supplementary Figure 4). Recent clinical study showed low sorafenib distribution in tumor tissues that contributed to its poor antitumor and antivascular activities [57]. Decreased penetration of sorafenib may be one of the mechanisms responsible for resistance, which warrants further study [8]. The antiproliferative response was enhanced when mixed-cell spheroids were treated with a combination of sorafenib and TEW-7197/pentoxifylline (Figure 5, *C* and *D*). The TGF-β1 receptor antagonist TEW-7197 has shown antifibrotic activity in preclinical studies and is being investigated in combination with chemotherapy in phase I clinical trials [58, 59]. The TGF-βR1 inhibitor LY2157299 is in clinical trials as a potential strategy to overcome sorafenib resistance (NCT01246986) [60]. The methylxanthine derivative pentoxifylline, which was initially used to treat peripheral vascular disease, also possesses antifibrotic activity either directly by increasing collagenase activity or indirectly by targeting TGF-β/CTGF signaling [61, 62]. We also observed the antifibrotic activity of both agents as demonstrated by reduced level of TGF-β/CTGF expression in the mixed-cell spheroids (Supplementary Figure 5).

After crossing the basement membrane, cancer cells degrade the stroma to enter blood or lymphatic vessels and finally metastasize to other organs [63]. 3D spheroids invasion in a matrix closely mimics cancer cell invasion under *in vivo* conditions and is widely utilized [20, 22]. Matrigel, collagen gels, and other human-derived matrix are utilized as ECM substrates in the *in vitro* invasion assays [64–66]. During tumor cells invasion, CAFs lead cancer cell invasion [67]. Fibroblast-led invasion was also demonstrated in the 3D cancer and fibroblasts co-culture studies [68, 69]. By embedding 3D spheroids in matrix (Matrigel and collagen), our mixed-cell spheroids was successfully used in evaluating HSC and HCC cell invasion. Cancer cell migration was significantly enhanced when HSCs were mixed in 3D spheroids (Figure 6, Supplementary Figure 3). Collective cell migration was seen as multicellular strands radiating from the periphery of mixed-cell spheroids. LX-2 cells were seen to lead this process, with matrix invasion observed after 24 hours in culture, whereas HCC cell migration was not yet detected (Figure 6*C*). After 48 and 72 hours, however, Huh-7 cell showed invasive movement, and both LX-2 and Huh-7 cells were seen in the migrating strand (Figure 6*C*). The proinvasive (filopodium and invadosomes) and EMT phenotype was observed in the mixed-cell spheroids even without matrix embedding (Figures 1*B* and 4*A*), supporting the active role of HSCs in stimulating motility of HCC cells (Figure 6*C*).

In summary, we developed a stroma-rich mixed-cell spheroid model by co-culturing HCC cells and HSCs in 96-well ULA plates. The tumor-stoma interactions maintained *via* juxtacrine and paracrine mechanisms were recapitulated in the present model. The similarity of mixed-cell spheroids with the *in vivo* tumor phenotype was confirmed by the profibrotic microenvironment and EMT phenotype including drug resistance and invasive cell movement. Our results also demonstrated the potential use of TGF-β1 inhibition in improving sorafenib efficacy. This mixed-cell spheroid model can be used to investigate crucial factors involved in EMT and to evaluate the potential agents to inhibit stroma-secreted factors and overcome drug resistance and tumor invasion.

Conflict of Interest

The authors declare no conflicts of interest.

Acknowledgements

This work was supported by the National Research Foundation of Korea (NRF) grants funded by the Korean Government (MEST) (NRF-2012R1A5A2047939 and NRF-2016R1A2B2011832).

Appendix A. Supplementary Data

Supplementary data to this article can be found online at https://doi.org/10.1016/j.neo.2018.05.008.

References

[1] El-Serag HB (2011). Hepatocellular carcinoma. *N Engl J Med* **365**, 1118–1127.
[2] Brown KS (2006). Chemotherapy and other systemic therapies for hepatocellular carcinoma and liver metastases. *Semin Intervent Radiol* **23**, 99–108.
[3] Waly Raphael S, Yangde Z, and Yuxiang C (2012). Hepatocellular carcinoma: focus on different aspects of management. *ISRN Oncol* **2012**, 421673.
[4] Deng GL, Zeng S, and Shen H (2015). Chemotherapy and target therapy for hepatocellular carcinoma: new advances and challenges. *World J Hepatol* **7**, 787–798.
[5] Llovet JM, Ricci S, Mazzaferro V, Hilgard P, Gane E, Blanc JF, de Oliveira AC, Santoro A, Raoul JL, and Forner A, et al (2008). Sorafenib in advanced hepatocellular carcinoma. *N Engl J Med* **359**, 378–390.
[6] Nishida N, Kitano M, Sakurai T, and Kudo M (2015). Molecular mechanism and prediction of sorafenib chemoresistance in human hepatocellular carcinoma. *Dig Dis* **33**, 771–779.
[7] Hanahan D and Coussens LM (2012). Accessories to the crime: functions of cells recruited to the tumor microenvironment. *Cancer Cell* **21**, 309–322.
[8] Khawar IA, Kim JH, and Kuh HJ (2015). Improving drug delivery to solid tumors: priming the tumor microenvironment. *J Control Release* **201**, 78–89.
[9] Hernandez-Gea V, Toffanin S, Friedman SL, and Llovet JM (2013). Role of the microenvironment in the pathogenesis and treatment of hepatocellular carcinoma. *Gastroenterology* **144**, 512–527.
[10] Leonardi GC, Candido S, Cervello M, Nicolosi D, Raiti F, Travali S, Spandidos DA, and Libra M (2012). The tumor microenvironment in hepatocellular carcinoma (review). *Int J Oncol* **40**, 1733–1747.
[11] Kubo N, Araki K, Kuwano H, and Shirabe K (2016). Cancer-associated fibroblasts in hepatocellular carcinoma. *World J Gastroenterol* **22**, 6841–6850.
[12] Affo S, Yu LX, and Schwabe RF (2017). The role of cancer-associated fibroblasts and fibrosis in liver cancer. *Annu Rev Pathol* **12**, 153–186.
[13] Carloni V, Luong TV, and Rombouts K (2014). Hepatic stellate cells and extracellular matrix in hepatocellular carcinoma: more complicated than ever. *Liver Int* **34**, 834–843.
[14] Coulouarn C and Clement B (2014). Stellate cells and the development of liver cancer: therapeutic potential of targeting the stroma. *J Hepatol* **60**, 1306–1309.

[15] Yang MC, Wang CJ, Liao PC, Yen CJ, and Shan YS (2014). Hepatic stellate cells secretes type I collagen to trigger epithelial mesenchymal transition of hepatoma cells. *Am J Cancer Res* **4**, 751–763.
[16] Mazzocca A, Fransvea E, Dituri F, Lupo L, Antonaci S, and Giannelli G (2010). Down-regulation of connective tissue growth factor by inhibition of transforming growth factor beta blocks the tumor-stroma cross-talk and tumor progression in hepatocellular carcinoma. *Hepatology* **51**, 523–534.
[17] He L, Tian DA, Li PY, and He XX (2015). Mouse models of liver cancer: progress and recommendations. *Oncotarget* **6**, 23306–23322.
[18] Coulouarn C, Corlu A, Glaise D, Guenon I, Thorgeirsson SS, and Clement B (2012). Hepatocyte-stellate cell cross-talk in the liver engenders a permissive inflammatory microenvironment that drives progression in hepatocellular carcinoma. *Cancer Res* **72**, 2533–2542.
[19] Weiswald LB, Bellet D, and Dangles-Marie V (2015). Spherical cancer models in tumor biology. *Neoplasia* **17**, 1–15.
[20] Takai A, Fako V, Dang H, Forgues M, Yu Z, Budhu A, and Wang XW (2016). Three-dimensional organotypic culture models of human hepatocellular carcinoma. *Sci Rep* **6**21174.
[21] van Zijl F and Mikulits W (2010). Hepatospheres: three dimensional cell cultures resemble physiological conditions of the liver. *World J Hepatol* **2**, 1–7.
[22] Song Y, Kim SH, Kim KM, Choi EK, Kim J, and Seo HR (2016). Activated hepatic stellate cells play pivotal roles in hepatocellular carcinoma cell chemoresistance and migration in multicellular tumor spheroids. *Sci Rep* **6**36750.
[23] Majety M, Pradel LP, Gies M, and Ries CH (2015). Fibroblasts influence survival and therapeutic response in a 3D co-culture model. *PLoS One* **10**e0127948.
[24] Ware MJ, Keshishian V, Law JJ, Ho JC, Favela CA, Rees P, Smith B, Mohammad S, Hwang RF, and Rajapakshe K, et al (2016). Generation of an in vitro 3D PDAC stroma rich spheroid model. *Biomaterials* **108**, 129–142.
[25] Jung HR, Kang HM, Ryu JW, Kim DS, Noh KH, Kim ES, Lee HJ, Chung KS, Cho HS, and Kim NS, et al (2017). Cell spheroids with enhanced aggressiveness to mimic human liver cancer in vitro and in vivo. *Sci Rep* **7**10499.
[26] Xu L, Hui AY, Albanis E, Arthur MJ, O'Byrne SM, Blaner WS, Mukherjee P, Friedman SL, and Eng FJ (2005). Human hepatic stellate cell lines, LX-1 and LX-2: new tools for analysis of hepatic fibrosis. *Gut* **54**, 142–151.
[27] Priwitaningrum DL, Blonde JG, Sridhar A, van Baarlen J, Hennink WE, Storm G, Le Gac S, and Prakash J (2016). Tumor stroma-containing 3D spheroid arrays: a tool to study nanoparticle penetration. *J Control Release* **244**, 257–268.
[28] An HJ, Jang JW, Bae SH, Choi JY, Cho SH, Yoon SK, Han JY, Lee KH, Kim DG, and Jung ES (2010). Sustained low hepatitis B viral load predicts good outcome after curative resection in patients with hepatocellular carcinoma. *J Gastroenterol Hepatol* **25**, 1876–1882.
[29] Ahmed SU, Zair M, Chen K, Iu M, He F, Adeyi O, Cleary SP, and Ghanekar A (2013). Generation of subcutaneous and intrahepatic human hepatocellular carcinoma xenografts in immunodeficient mice. *J Vis Exp* e50544.
[30] Friedrich J, Eder W, Castaneda J, Doss M, Huber E, Ebner R, and Kunz-Schughart LA (2007). A reliable tool to determine cell viability in complex 3-d culture: the acid phosphatase assay. *J Biomol Screen* **12**, 925–937.
[31] Di Veroli GY, Fornari C, Goldlust I, Mills G, Koh SB, Bramhall JL, Richards FM, and Jodrell DI (2015). An automated fitting procedure and software for dose-response curves with multiphasic features. *Sci Rep* **5**14701.
[32] Vinci M, Box C, and Eccles SA (2015). Three-dimensional (3D) tumor spheroid invasion assay. *J Vis Exp* e52686.
[33] Park SA, Kim MJ, Park SY, Kim JS, Lim W, Nam JS, and Yhong Sheen Y (2015). TIMP-1 mediates TGF-beta-dependent crosstalk between hepatic stellate and cancer cells via FAK signaling. *Sci Rep* **5**16492.
[34] Breslin S and O'Driscoll L (2016). The relevance of using 3D cell cultures, in addition to 2D monolayer cultures, when evaluating breast cancer drug sensitivity and resistance. *Oncotarget* **7**, 45745–45756.
[35] Krelle Ann C, Okoli Arinze S, and Mendz George L (2013). Huh-7 human liver cancer cells: a model system to understand hepatocellular carcinoma and therapy. *J Cancer Ther* **4**, 606–631.
[36] Chen B, Sirota M, Fan-Minogue H, Hadley D, and Butte AJ (2015). Relating hepatocellular carcinoma tumor samples and cell lines using gene expression data in translational research. *BMC Med Genet* **2**(8 Suppl), S5.
[37] Kim EY and Kim AK (2012). Apigenin sensitizes Huh-7 human hepatocellular carcinoma cells to TRAIL-induced apoptosis. *Biomol Ther* **20**, 62–67.
[38] Yip D and Cho CH (2013). A multicellular 3D heterospheroid model of liver tumor and stromal cells in collagen gel for anti-cancer drug testing. *Biochem Biophys Res Commun* **433**, 327–332.
[39] Costa EC, Moreira AF, de Melo-Diogo D, Gaspar VM, Carvalho MP, and Correia IJ (2016). 3D tumor spheroids: an overview on the tools and techniques used for their analysis. *Biotechnol Adv* **34**, 1427–1441.
[40] Shi YF, Fong CC, Zhang Q, Cheung PY, Tzang CH, Wu RS, and Yang M (2007). Hypoxia induces the activation of human hepatic stellate cells LX-2 through TGF-beta signaling pathway. *FEBS Lett* **581**, 203–210.
[41] LaGory EL and Giaccia AJ (2016). The ever-expanding role of HIF in tumour and stromal biology. *Nat Cell Biol* **18**, 356–365.
[42] Friedman SL (2008). Hepatic stellate cells: protean, multifunctional, and enigmatic cells of the liver. *Physiol Rev* **88**, 125–172.
[43] Xiu M, Liu YH, Brigstock DR, He FH, Zhang RJ, and Gao RP (2012). Connective tissue growth factor is overexpressed in human hepatocellular carcinoma and promotes cell invasion and growth. *World J Gastroenterol* **18**, 7070–7078.
[44] Urtasun R, Latasa MU, Demartis MI, Balzani S, Goni S, Garcia-Irigoyen O, Elizalde M, Azcona M, Pascale RM, and Feo F, et al (2011). Connective tissue growth factor autocriny in human hepatocellular carcinoma: oncogenic role and regulation by epidermal growth factor receptor/yes-associated protein-mediated activation. *Hepatology* **54**, 2149–2158.
[45] Parikh JG, Kulkarni A, and Johns C (2014). Alpha-smooth muscle actin-positive fibroblasts correlate with poor survival in hepatocellular carcinoma. *Oncol Lett* **7**, 573–575.
[46] Chao C, Widen SG, Wood TG, Zatarain JR, Johnson P, Gajjar A, Gomez G, Qiu S, Thompson J, and Spratt H, et al (2017). Patient-derived xenografts from colorectal carcinoma: a temporal and hierarchical study of murine stromal sell replacement. *Anticancer Res* **37**, 3405–3412.
[47] Maykel J, Liu JH, Li H, Shultz LD, Greiner DL, and Houghton J (2014). NOD-scidIl2rg (tm1Wjl) and NOD-Rag1 (null) Il2rg (tm1Wjl) : a model for stromal cell-tumor cell interaction for human colon cancer. *Dig Dis Sci* **59**, 1169–1179.
[48] Kang N, Gores GJ, and Shah VH (2011). Hepatic stellate cells: partners in crime for liver metastases? *Hepatology* **54**, 707–713.
[49] Giannelli G, Villa E, and Lahn M (2014). Transforming growth factor-beta as a therapeutic target in hepatocellular carcinoma. *Cancer Res* **74**, 1890–1894.
[50] Kim EJ, Kim HJ, Park MK, Kang GJ, Byun HJ, Lee H, and Lee CH (2015). Cardamonin suppresses TGF-beta1-induced epithelial mesenchymal transition via restoring protein phosphatase 2A expression. *Biomol Ther* **23**, 141–148.
[51] Kim SH, Choi SJ, Kim YC, and Kuh HJ (2009). Anti-tumor activity of noble indirubin derivatives in human solid tumor models in vitro. *Arch Pharm Res* **32**, 915–922.
[52] Lee SH, Nam JK, Park JK, Lee JH, Min do S, and Kuh HJ (2014). Differential protein expression and novel biomarkers related to 5-FU resistance in a 3D colorectal adenocarcinoma model. *Oncol Rep* **32**, 1427–1434.
[53] Zeng F, Ju R-J, Li X-T, and Lu W-L (2014). Advances in investigations on the mechanism of cancer multidrug resistance and the liposomes-based treatment strategy. *J Pharm Investig* **44**, 493–504.
[54] Song Y, Kim JS, Choi EK, Kim J, Kim KM, and Seo HR (2017). TGF-beta-independent CTGF induction regulates cell adhesion mediated drug resistance by increasing collagen I in HCC. *Oncotarget* **8**, 21650–21662.
[55] Wang Z, Zhou J, Fan J, Qiu SJ, Yu Y, Huang XW, Sun J, Tan CJ, and Dai Z (2009). Oxaliplatin induces apoptosis in hepatocellular carcinoma cells and inhibits tumor growth. *Expert Opin Investig Drugs* **18**, 1595–1604.
[56] Petrelli F, Coinu A, Borgonovo K, Cabiddu M, Ghilardi M, Lonati V, and Barni S (2014). Oxaliplatin-based chemotherapy: a new option in advanced hepatocellular carcinoma. a systematic review and pooled analysis. *Clin Oncol* **26**, 488–496.
[57] Torok S, Rezeli M, Kelemen O, Vegvari A, Watanabe K, Sugihara Y, Tisza A, Marton T, Kovacs I, and Tovari J, et al (2017). Limited tumor tissue drug penetration contributes to primary resistance against angiogenesis inhibitors. *Theranostics* **7**, 400–412.
[58] Jin CH, Krishnaiah M, Sreenu D, Subrahmanyam VB, Rao KS, Lee HJ, Park SJ, Park HJ, Lee K, and Sheen YY, et al (2014). Discovery of N-((4-([1,2,4]triazolo[1,5-a]pyridin-6-yl)-5-(6-methylpyridin-2-yl)-1H-imidazol-2-yl)methyl)-2-fluoroaniline (EW-7197): a highly potent, selective, and orally bioavailable inhibitor of TGF-beta type I receptor kinase as cancer immunotherapeutic/antifibrotic agent. *J Med Chem* **57**, 4213–4238.
[59] Park SA, Kim MJ, Park SY, Kim JS, Lee SJ, Woo HA, Kim DK, Nam JS, and Sheen YY (2015). EW-7197 inhibits hepatic, renal, and pulmonary fibrosis by blocking TGF-beta/Smad and ROS signaling. *Cell Mol Life Sci* **72**, 2023–2039.
[60] Serova M, Tijeras-Raballand A, Dos Santos C, Albuquerque M, Paradis V, Neuzillet C, Benhadji KA, Raymond E, Faivre S, and de Gramont A (2015). Effects of TGF-beta signalling inhibition with galunisertib (LY2157299) in hepatocellular carcinoma models and in ex vivo whole tumor tissue samples from patients. *Oncotarget* **6**, 21614–21627.

[61] Lin SL, Chen RH, Chen YM, Chiang WC, Lai CF, Wu KD, and Tsai TJ (2005). Pentoxifylline attenuates tubulointerstitial fibrosis by blocking Smad3/4-activated transcription and profibrogenic effects of connective tissue growth factor. *J Am Soc Nephrol* **16**, 2702–2713.

[62] Kim JH, Shin BC, Park WS, Lee J, and Kuh HJ (2017). Antifibrotic effects of pentoxifylline improve the efficacy of gemcitabine in human pancreatic tumor xenografts. *Cancer Sci* **108**, 2470–2477.

[63] Clark AG and Vignjevic DM (2015). Modes of cancer cell invasion and the role of the microenvironment. *Curr Opin Cell Biol* **36**, 13–22.

[64] Kleinman HK and Martin GR (2005). Matrigel: basement membrane matrix with biological activity. *Semin Cancer Biol* **15**, 378–386.

[65] Wolf K, Alexander S, Schacht V, Coussens LM, von Andrian UH, van Rheenen J, Deryugina E, and Friedl P (2009). Collagen-based cell migration models in vitro and in vivo. *Semin Cell Dev Biol* **20**, 931–941.

[66] Salo T, Sutinen M, Hoque Apu E, Sundquist E, Cervigne NK, de Oliveira CE, Akram SU, Ohlmeier S, Suomi F, and Eklund L, et al (2015). A novel human leiomyoma tissue derived matrix for cell culture studies. *BMC Cancer* **15**, 981.

[67] Gaggioli C, Hooper S, Hidalgo-Carcedo C, Grosse R, Marshall JF, Harrington K, and Sahai E (2007). Fibroblast-led collective invasion of carcinoma cells with differing roles for RhoGTPases in leading and following cells. *Nat Cell Biol* **9**, 1392–1400.

[68] Attieh Y, Clark AG, Grass C, Richon S, Pocard M, Mariani P, Elkhatib N, Betz T, Gurchenkov B, and Vignjevic DM (2017). Cancer-associated fibroblasts lead tumor invasion through integrin-beta3-dependent fibronectin assembly. *J Cell Biol* **216**, 3509–3520.

[69] Dang TT, Prechtl AM, and Pearson GW (2011). Breast cancer subtype-specific interactions with the microenvironment dictate mechanisms of invasion. *Cancer Res* **71**, 6857–6866.